ACADÉMIE
DES SCIENCES
INSTITUT DE FRANCE

Comptes Rendus
Physique

Franck Plunian, Paul Gomez and Thierry Alboussière

Three-body anisotropic dynamo: the rotor, the gap and the stator

Volume 26 (2025), p. 295-315

Online since: 26 March 2025

https://doi.org/10.5802/crphys.245

CENTRE MERSENNE
The Comptes Rendus. Physique *are a member of the Mersenne Center for open scientific publishing*
www.centre-mersenne.org — e-ISSN : 1878-1535

ACADÉMIE
DES SCIENCES
INSTITUT DE FRANCE

Comptes Rendus. Physique
2025, Vol. 26, p. 295-315
https://doi.org/10.5802/crphys.245

Research article / *Article de recherche*

Three-body anisotropic dynamo: the rotor, the gap and the stator

Dynamo anisotrope à trois corps : le rotor, l'entrefer et le stator

Franck Plunian [*, a], **Paul Gomez** [b] and **Thierry Alboussière** [b]

[a] Univ. Grenoble Alpes, Univ. Savoie Mont Blanc, CNRS, IRD, Univ. Gustave Eiffel, ISTerre, 38000 Grenoble, France

[b] Université Lyon 1, ENS de Lyon, CNRS, Laboratoire de Géologie de Lyon, Lyon 69622, France

E-mails: Franck.Plunian@univ-grenoble-alpes.fr (F. Plunian), paul.gomez@ens-lyon.fr (P. Gomez), thierry.alboussiere@ens-lyon.fr (T. Alboussière)

Abstract. Following the success of the experimental Fury dynamo [1], we are studying (i) the possibility of a new experiment with the same geometry and the same anisotropic electrical conductivity, but with a wider galinstan gap between the rotor and the stator than in Fury, in order to allow richer dynamics via Lorentz forces. Of course, to do this, we must first be able to start the dynamo with a large gap, which is the first objective of this study. The second objective (ii) is to design a miniature dynamo experiment, smaller than Fury, and with a narrow gap comparable to that of Fury. The use this time of anisotropic magnetic permeability instead of anisotropic electrical conductivity is the most appropriate solution. Theory shows that without a gap, using one rather than the other does not change the threshold of the dynamo, and only the direction of rotation of the rotor has to be reversed [2]. With a gap filled with galinstan, even a very narrow one, and unlike Fury whose rotor and stator were mainly made of copper, here the use of iron leads to a significant jump in magnetic permeability with galinstan, which could be detrimental to the dynamo. In order to study these two issues relating to (i) the thickness of the gap, and (ii) the electromagnetic properties of the material filling the gap compared with those of the rotor and stator, we need to solve the problem of the three-body anisotropic dynamo: the rotor, the gap and the stator.

Résumé. Suite au succès de la dynamo expérimentale Fury [1], nous étudions (i) la possibilité d'une nouvelle expérience avec la même géométrie et la même conductivité électrique anisotrope, mais avec un entrefer de galinstan entre le rotor et le stator plus large que dans Fury, afin de permettre une dynamique plus riche via les forces de Lorentz. Bien sûr, pour ce faire, nous devons d'abord être en mesure de démarrer la dynamo avec un large entrefer, ce qui constitue le premier objectif de cette étude. Le deuxième objectif (ii) est de concevoir une expérience de dynamo miniature, plus petite que Fury, et avec un entrefer étroit, comparable à celui de Fury. L'utilisation cette fois d'une perméabilité magnétique anisotrope au lieu d'une conductivité électrique anisotrope est la solution la plus appropriée. La théorie montre que sans entrefer, l'utilisation de l'une plutôt que l'autre ne change pas le seuil de la dynamo, et seul le sens de rotation du rotor doit être inversé [2]. Avec un entrefer rempli de galinstan, même très étroit et contrairement à Fury dont le rotor et le stator étaient principalement constitués de cuivre, ici l'utilisation de fer entraîne un saut significatif de perméabilité magnétique avec le galinstan, ce qui pourrait être préjudiciable à la dynamo. Pour étudier ces deux questions liées (i) à l'épaisseur de l'entrefer, et (ii) aux propriétés électromagnétiques du matériau remplissant l'entrefer

* Corresponding author

par rapport à celles du rotor et du stator, nous devons résoudre le problème de la dynamo anisotrope à trois corps : le rotor, l'entrefer et le stator.

Keywords. Dynamo effect, Anisotropic electromagnetic properties, Dynamo experiment.

Mots-clés. Effet dynamo, Propriétés électromagnétiques anisotropes, Dynamo expérimentale.

Funding. French Academy of Sciences and Electricité de France, PEPR Origins.

Manuscript received 18 December 2024, revised and accepted 7 March 2025.

1. Introduction

The Fury experiment demonstrated that it was possible to produce a dynamo effect using a material with anisotropic electrical conductivity [1]. Such material was obtained by alternating layers of copper and kapton in order to favour electrical currents along the copper layers and slow them down in the direction perpendicular to the layers. Fury's geometry consists of a cylindrical rotor rotating inside a cylindrical stator, both made with this copper/kapton material, and a thin gap between the rotor and stator, filled with galinstan to ensure good electrical contact between the two solid parts (see Figure 2).

In Fury, the gap is so thin that even if the galinstan flow is turbulent, with a Reynolds number of about 5000, it plays no other role than to ensure good electric contact between the rotor and the stator, which is why it is neglected in the theoretical models [2]. Above the dynamo threshold, the additional mechanical power injected is then entirely dissipated in the form of Joule dissipation, and the magnetic field has no dynamic behaviour other than saturation. This contrasts with fluid dynamo experiments in which the additional mechanical power is mainly dissipated in the form of turbulent hydrodynamic dissipation [3–5], and for which the magnetic field generated can be dynamically unstable, with chaotic or cyclic behaviour [6], similar to the magnetic field observed at the surface of the Earth or the Sun.

The advantage of Fury is that it is relatively small, inexpensive, and avoids the use of liquid sodium, which requires an appropriate safety environment. Therefore, it could be interesting to study a new experimental configuration, similar to Fury but with a larger galinstan gap so that the system benefits from the advantages of Fury as well as from a larger number of degrees of freedom that could potentially lead to dynamical instabilities. Although the role of small-scale turbulence in the fluid may be crucial in the dynamo process, presumably leading to additional magnetic dissipation in the fluid, it is reasonable to start with a simple solid-body rotation for the fluid motion in the gap. Such simple configuration has also the advantage to be mathematically tractable. It can even be approximated to be at rest, at least for some time after the rotor has started to rotate, with Stewartson boundary layers at the lateral wall of the rotor, sufficiently thin to be ignored. Theoretically, we expect the dynamo threshold to increase with the thickness of the gap. It is therefore necessary to solve a three-body problem, consisting of two anisotropic bodies separated by a gap filled with an isotropic material. This is the first objective of this paper. We note that the limiting case of an infinite gap (without stator) has already being studied [7]. It corresponds to a two-body system, consisting of an anisotropic rotor immersed in an isotropic medium (e.g. a liquid metal). In this case the dynamo threshold is higher than in Fury, requiring a larger rotor size and also a large quantity of liquid metal around it. This configuration has been suggested as a good candidate for starting a dynamo in large installations such as those built in Maryland, Wisconsin or Dresden [8,9].

The three-body anisotropic dynamo is also crucial to study in the case where the presence of a galinstan gap has an effect on the dynamo's threshold not because of its thickness but because of the difference in electromagnetic properties between the liquid metal filling the gap and the materials making up the rotor and stator. In Fury, although the electrical conductivity ratio between galinstan and copper is small, around 6×10^{-2}, the presence of a thin galinstan gap does not significantly alter the dynamo threshold. On the other hand, if we use a rotor and stator with an anisotropic magnetic permeability instead of an anisotropic electric conductivity, the difference in magnetic permeability with galinstan can be significantly lower and potentially be much more detrimental to the dynamo. By way of comparison, the magnetic permeability ratio between galinstan and soft iron is around 2×10^{-4}, the one between galinstan and μ-metal is around 6.7×10^{-6} (see Table 1). This is all the more interesting because, if we neglect the presence of the gap, the dynamo threshold for a rotor and stator made of soft iron (resp. μ-metal) and tin is around a hundred (resp. thousand) times smaller than Fury's, made of copper and kapton, suggesting the possibility of building a miniature dynamo. In fact, the degree of miniaturisation will depend on the effect of the jump in magnetic permeability between galinstan filling the gap and soft iron (resp. μ-metal). In terms of miniaturisation, Fury's net mass (without infrastructure) is around 43 kg, while the Maryland and Dresden experiments exceed 14 tonnes and 6 tonnes respectively. We are aiming here for an experiment net mass of around 1 kg.

Last but not least, in order to construct a stator and rotor with an anisotropic electric conductivity (resp. magnetic permeability), an alternation of two materials is necessary, in order to constrain the electric currents (resp. the magnetic field). Then, this study seems in line with previous dynamo studies underlining the benefic action of inhomogeneous materials [10–14]. However, from a theoretical point of view, the anisotropic dynamo only relies on anisotropy, and not on inhomogeneity. To illustrate this point, the corresponding dynamo mechanism is illustrated in Figure 1 in cartesian geometry. In an appropriate reference frame, the shear between two moving parts of a single homogeneous material is represented by the two opposite velocities $\boldsymbol{U}$. We assume that the electrical conductivity is maximum along vertical planes parallel to the fine lines drawn at the top horizontal surfaces. These lines are here only to fix the eye, the material then staying homogeneous, but with an anisotropic electrical conductivity. We note that these lines are not perpendicular to $\boldsymbol{U}$, implying that the horizontal component of the electric current density $\boldsymbol{J}$ is not perpendicular to $\boldsymbol{U}$ either. Considering a current density loop as represented in red in Figure 1, the magnetic field $\boldsymbol{B}$ which is induced by $\boldsymbol{J}$ has a component perpendicular to $\boldsymbol{U}$, such that $\boldsymbol{U} \times \boldsymbol{B} \neq 0$ (Ohm's law) reinforces the vertical component of $\boldsymbol{J}$. This illustrates the dynamo mechanism, provided $\boldsymbol{U}$ is sufficiently large. On the other hand, if $\boldsymbol{U}$ is changed in $-\boldsymbol{U}$, or equivalently if the direction of the anisotropy α is changed in $-\alpha$, then $\boldsymbol{U} \times \boldsymbol{B}$ will be opposite and then will weaken the vertical component of $\boldsymbol{J}$, making the dynamo impossible. If the electrical conductivity is isotropic, then the current loop will follow the shortest way which is in planes perpendicular to $\boldsymbol{U}$. In that case, the induced magnetic field $\boldsymbol{B}$ becomes parallel to $\boldsymbol{U}$ and then unable to drive a current density, as $\boldsymbol{U} \times \boldsymbol{B} = 0$.

In Section 2, the configuration of the three-body problem is introduced as well as the set of equations to be solved. In Section 3 the boundary conditions are presented, followed by a renormalisation of the problem leading to dimensionless variables. In Section 4, a dispersion relation is derived, and an explicit expression for the magnetic Reynolds number is given, followed in section 5 by significant results, dimensionless and dimensional.

2. General formulation

As shown in Figure 2, we consider three cylindrical bodies, the rotor ($r < R$), the gap ($R < r < R+e$) and the stator ($r > R + e$), where r is the radial coordinate in cylindrical geometry. The rotor rotates with a solid body rotation given by the angular velocity Ω, while the stator is at rest. The gap in between can also rotate, with an angular velocity ω which, for mathematical convenience,

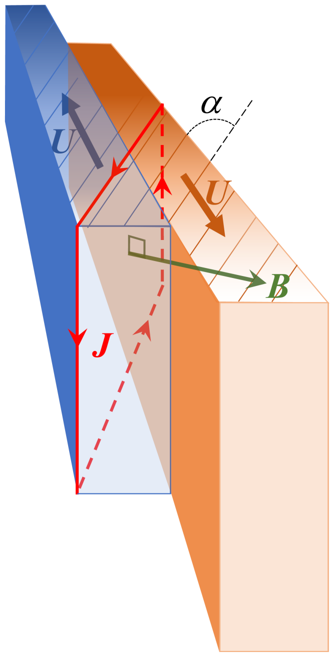

Figure 1. Illustration of the anisotropic dynamo mechanism. The two moving parts are made of the same homogeneous material. The maximum electrical conductivity is along vertical planes parallel to the lines drawn at the top surfaces. The current density loop $\boldsymbol{J}$ (in red) induces a magnetic field $\boldsymbol{B}$ (in green). The component of $\boldsymbol{B}$ which is perpendicular to $\boldsymbol{U}$ reinforces the vertical component of $\boldsymbol{J}$ in each moving part, through the cross product $\boldsymbol{U}\times\boldsymbol{B}$ (Ohm's law), making the dynamo possible (provided a velocity threshold is exceeded to compensate for Joule dissipation).

is considered to be also constant in r (solid body rotation), with $\omega\in[0,\Omega]$. The velocity field is then given by

$$\boldsymbol{U}=r\tilde{\Omega}\boldsymbol{e}_\theta,\quad \text{with } \tilde{\Omega}=\begin{cases}\Omega, & 0<r<R\\ \omega, \quad \text{for} & R<r<R+e\\ 0, & r>R+e,\end{cases} \tag{1}$$

where $(\boldsymbol{e}_r,\boldsymbol{e}_\theta,\boldsymbol{e}_z)$ and (r,θ,z) are unit basis vectors and coordinates in cylindrical geometry.

The electrical conductivity and magnetic permeability of the rotor and stator have the same anisotropy. We define the electrical conductivity and the magnetic permeability by $\sigma^{\parallel}$ and $\mu^{\parallel}$ in a given direction $\boldsymbol{q}$, and by $\sigma^{\perp}$ and $\mu^{\perp}$ in the directions perpendicular to $\boldsymbol{q}$, where $\boldsymbol{q}$ is a unit vector. In the direction parallel to $\boldsymbol{q}$, Ohm's law and the relation between $\boldsymbol{H}$ and $\boldsymbol{B}$ are written in the form $\boldsymbol{J}\cdot\boldsymbol{q}=\sigma^{\parallel}(\boldsymbol{E}\cdot\boldsymbol{q})$ and $\boldsymbol{B}\cdot\boldsymbol{q}=\mu^{\parallel}(\boldsymbol{H}\cdot\boldsymbol{q})$, while in the directions perpendicular to $\boldsymbol{q}$, they are written as $\boldsymbol{J}-(\boldsymbol{J}\cdot\boldsymbol{q})\boldsymbol{q}=\sigma^{\perp}(\boldsymbol{E}-(\boldsymbol{E}\cdot\boldsymbol{q})\boldsymbol{q})$ and $\boldsymbol{B}-(\boldsymbol{B}\cdot\boldsymbol{q})\boldsymbol{q}=\mu^{\perp}(\boldsymbol{H}-(\boldsymbol{H}\cdot\boldsymbol{q})\boldsymbol{q})$. This leads to two symmetric tensors, $[\sigma_{ij}]$ for the electrical conductivity and $[\mu_{ij}]$ for the magnetic permeability, defined by [15]

$$[\sigma_{ij}]=\sigma^{\perp}\delta_{ij}+(\sigma^{\parallel}-\sigma^{\perp})q_iq_j,\quad [\mu_{ij}]=\mu^{\perp}\delta_{ij}+(\mu^{\parallel}-\mu^{\perp})q_iq_j. \tag{2a,b}$$

The expressions (2a,b) also encompass the isotropic electromagnetic properties of the fluid in the gap, σ_g and μ_g, replacing $\sigma^{\perp}$ and $\sigma^{\parallel}$ by σ_g, $\mu^{\perp}$ and $\mu^{\parallel}$ by μ_g. Anticipating a renormalisation

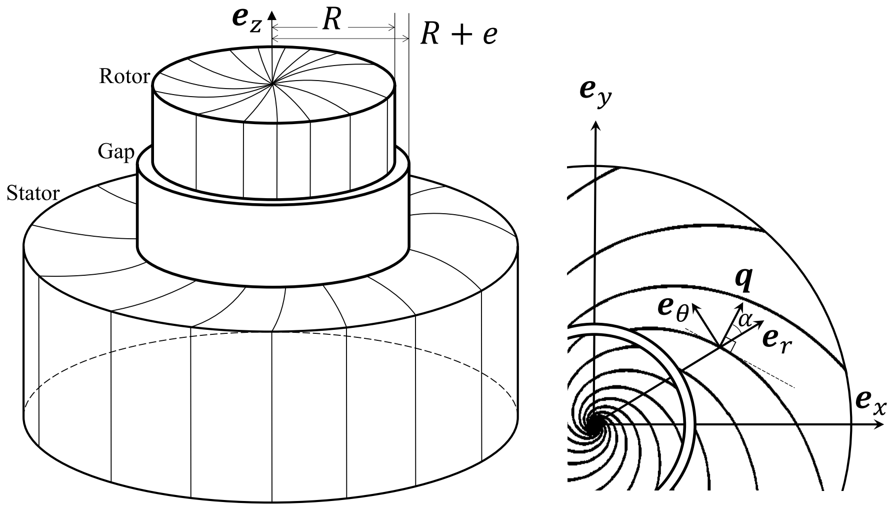

Figure 2. Left: Exploded view of the rotor surrounded by the gap, itself surrounded by the stator. Right: The logarithmic spirals in the rotor and stator correspond to the direction of the electric current (resp. magnetic field) for $\sigma^\perp \gg \sigma^\parallel$ (resp. $\mu^\perp \gg \mu^\parallel$), in the horizontal plane seen from above. They are perpendicular to $\boldsymbol{q}$.

of the electrical conductivity and magnetic permeability by $\sigma^\perp$ and $\mu^\perp$, it is then useful to rewrite (2a,b) as following,

$$[\sigma_{ij}] = \sigma^\perp\, \tilde{\varphi}_\sigma \left(\delta_{ij} - \frac{\tilde{\sigma}}{1+\tilde{\sigma}} q_i q_j\right), \quad [\mu_{ij}] = \mu^\perp\, \tilde{\varphi}_\mu \left(\delta_{ij} - \frac{\tilde{\mu}}{1+\tilde{\mu}} q_i q_j\right), \tag{3a,b}$$

with

$$\tilde{\varphi}_\sigma = \begin{cases} 1 \\ \varphi_\sigma \\ 1, \end{cases} \quad \tilde{\sigma} = \begin{cases} \sigma \\ 0 \\ \sigma, \end{cases} \quad \tilde{\varphi}_\mu = \begin{cases} 1 \\ \varphi_\mu \\ 1, \end{cases} \quad \tilde{\mu} = \begin{cases} \mu & r < R \\ 0 \quad \text{for} & R < r < R+e \\ \mu & r > R+e, \end{cases} \tag{4a–d}$$

and

$$\varphi_\sigma = \frac{\sigma_g}{\sigma^\perp}, \quad \sigma = \frac{\sigma^\perp}{\sigma^\parallel} - 1, \quad \varphi_\mu = \frac{\mu_g}{\mu^\perp}, \quad \mu = \frac{\mu^\perp}{\mu^\parallel} - 1. \tag{5a–d}$$

As in [2,7,16,17], we choose $\boldsymbol{q}$ as a unit vector in the horizontal plane defined by

$$\boldsymbol{q} = c\, \boldsymbol{e}_r + s\, \boldsymbol{e}_\theta, \tag{6}$$

where $c = \cos\alpha$, $s = \sin\alpha$, with α a prescribed pitch angle. The vector $\boldsymbol{q}$ follows the direction of logarithmic spirals which are perpendicular to the ones shown in Figure 2 (see [18] for an alternative expression in cartesian geometry).

In the magnetohydrodynamic approximation, Maxwell's equations and Ohm's law take the following forms

$$\boldsymbol{H} = [\mu_{ij}]^{-1}\boldsymbol{B}, \tag{7a}$$

$$\nabla\cdot\boldsymbol{B} = 0, \tag{7b}$$

$$\boldsymbol{J} = \nabla\times\boldsymbol{H}, \tag{7c}$$

$$\partial_t \boldsymbol{B} = -\nabla\times\boldsymbol{E} \tag{7d}$$

$$\boldsymbol{J} = [\sigma_{ij}](\boldsymbol{E} + \boldsymbol{U}\times\boldsymbol{B}), \tag{7e}$$

leading to the equation for the magnetic induction $\boldsymbol{B}$,

$$\partial_t \boldsymbol{B} = \nabla \times (\boldsymbol{U} \times \boldsymbol{B}) - \nabla \times ([\sigma_{ij}]^{-1} \nabla \times ([\mu_{ij}]^{-1} \boldsymbol{B})), \tag{8}$$

where

$$[\sigma_{ij}]^{-1} = (\tilde{\varphi}_\sigma \sigma^\perp)^{-1}(\delta_{ij} + \tilde{\sigma} q_i q_j), \quad [\mu_{ij}]^{-1} = (\tilde{\varphi}_\mu \mu^\perp)^{-1}(\delta_{ij} + \tilde{\mu} q_i q_j). \tag{9a,b}$$

Equations (9a,b) are derived from (3a,b) knowing that, for any unit vector $\boldsymbol{q}$ and any scalar quantity $X \neq -1$, we have

$$\left[\delta_{ij} - \frac{X}{1+X} q_i q_j\right]^{-1} = \delta_{ij} + X q_i q_j. \tag{10}$$

Since the velocity is stationary and independent of z, and as we are considering only axisymmetric solutions, because they are the least dissipative ones and then likely to be dominant at the dynamo onset, we look for a magnetic induction in the form

$$\boldsymbol{B} = \boldsymbol{B}(r) \exp(\gamma t + \mathrm{i} k z), \tag{11}$$

where $\boldsymbol{B}(r)$ is the axisymmetric magnetic mode at vertical wave number k. In (11) a positive value of the real part of the magnetic growth rate γ is the signature of dynamo action. The dynamo threshold that we will be sought, corresponds to $\Re\{\gamma\} = 0$.

Replacing (1) and (11) in (8), and after some algebra (see e.g. [7]), one obtains the following equations for $B_r(r)$ and $B_\theta(r)$,

$$\tilde{\gamma} B_r = -(\sigma^\perp \mu^\perp)^{-1}[\tilde{\mu} c^2 k^2 B_r + (1 + \tilde{\sigma} s^2) D_k(B_r) - cs(\tilde{\sigma} - \tilde{\mu}) k^2 B_\theta], \tag{12a}$$

$$\tilde{\gamma} B_\theta = -(\sigma^\perp \mu^\perp)^{-1}[\tilde{\sigma} c^2 k^2 B_\theta + (1 + \tilde{\mu} s^2) D_k(B_\theta) - cs(\tilde{\sigma} - \tilde{\mu}) D_k(B_r)], \tag{12b}$$

where

$$\tilde{\gamma} = \tilde{\varphi}_\sigma \tilde{\varphi}_\mu \gamma = \begin{cases} \gamma, & r < R \\ \varphi_\sigma \varphi_\mu \gamma, \quad \text{for} & R < r < R + e \\ \gamma, & r > R + e \end{cases} \tag{13}$$

and

$$D_k(X) = k^2 X - \frac{\partial}{\partial r}\left(\frac{1}{r}\frac{\partial}{\partial r}(rX)\right). \tag{14}$$

3. Boundary conditions and renormalization

The system of Equations (12a,b) is completed by the appropriate boundary conditions for $r = 0$ and $r \to \infty$,

$$B_r(r=0) = B_\theta(r=0) = \lim_{r\to\infty} B_r = \lim_{r\to\infty} B_\theta = 0, \tag{15a–d}$$

and by the continuity across $r = R$ and $r = R + e$ of the normal component of $\boldsymbol{B}$ and of the tangential components of $\boldsymbol{H}$ and $\boldsymbol{E}$,

$$[B_r]_{R^-}^{R^+} = [H_\theta]_{R^-}^{R^+} = [H_z]_{R^-}^{R^+} = [E_\theta]_{R^-}^{R^+} = [E_z]_{R^-}^{R^+} = 0, \tag{16a–e}$$

$$[B_r]_{(R+e)^-}^{(R+e)^+} = [H_\theta]_{(R+e)^-}^{(R+e)^+} = [H_z]_{(R+e)^-}^{(R+e)^+} = [E_\theta]_{(R+e)^-}^{(R+e)^+} = [E_z]_{(R+e)^-}^{(R+e)^+} = 0, \tag{17a–e}$$

where $[X]_{r_1}^{r_2} = X(r = r_2) - X(r = r_1)$.

From (7a) and (9b), the magnetic field $\boldsymbol{H}$ takes the form

$$\boldsymbol{H} = (\tilde{\varphi}_\mu \mu^\perp)^{-1} \begin{pmatrix} (1 + \tilde{\mu} c^2) B_r + \tilde{\mu} cs B_\theta \\ \tilde{\mu} cs B_r + (1 + \tilde{\mu} s^2) B_\theta \\ B_z \end{pmatrix}, \tag{18}$$

with, from (7b),

$$B_z = \mathrm{i} k^{-1} \left(\frac{B_r}{r} + \frac{\partial B_r}{\partial r}\right). \tag{19}$$

Then (16a–c) and (17a–c) can be rewritten as

$$B_r(R^+) = B_r(R^-) \tag{20}$$

$$\varphi_\mu^{-1} B_\theta(R^+) = \mu c s B_r(R^-) + (1+\mu s^2) B_\theta(R^-) \tag{21}$$

$$\varphi_\mu^{-1}\left(\frac{B_r(R^+)}{R} + \frac{\partial B_r}{\partial r}(R^+)\right) = \frac{B_r(R^-)}{R} + \frac{\partial B_r}{\partial r}(R^-) \tag{22}$$

$$B_r((R+e)^-) = B_r((R+e)^+) \tag{23}$$

$$\varphi_\mu^{-1} B_\theta((R+e)^-) = \mu c s B_r((R+e)^+) + (1+\mu s^2) B_\theta((R+e)^+) \tag{24}$$

$$\varphi_\mu^{-1}\left(\frac{B_r((R+e)^-)}{(R+e)} + \frac{\partial B_r}{\partial r}((R+e)^-)\right) = \frac{B_r((R+e)^+)}{(R+e)} + \frac{\partial B_r}{\partial r}((R+e)^+). \tag{25}$$

From (7d) we have $E_\theta = -\mathrm{i}k^{-1}\gamma B_r$, implying that the two conditions (16a) and (16d) are redundant, as well as (17a) and (17d). As for the last boundary conditions (16e) and (17e), using (7e) we have

$$\tilde{\varphi}_\sigma^{-1} J_z + \sigma^\perp r \tilde{\Omega} B_r = \sigma^\perp E_z \tag{26}$$

with $\tilde{\Omega}$ defined in (1), leading to

$$\varphi_\sigma^{-1} J_z(R^+) + \sigma^\perp \omega R B_r(R^+) = J_z(R^-) + \sigma^\perp \Omega R B_r(R^-), \tag{27}$$

$$J_z((R+e)^+) = \varphi_\sigma^{-1} J_z((R+e)^-) + \sigma^\perp \omega (R+e) B_r((R+e)^-). \tag{28}$$

Renormalizing the distance and time by R and $\mu^\perp \sigma^\perp R^2$, and the current density $\boldsymbol{J}$ by $(\mu^\perp R)^{-1}$, corresponds to replacing R, $\sigma^\perp$ and $\mu^\perp$ by unity in the system (12a,b) and in the boundary conditions (16a–e), (17a–e), (20)–(25) and (27)–(28). Then the absolute value of the dimensionless angular velocity $|\Omega|$ corresponds to the magnetic Reynolds number. For the sake of simplicity, we will retain the notation e for the now-normalised thickness of the gap.

4. Resolution

As we are interested in the dynamo threshold, the system (12a,b) is solved for $\gamma = 0$, in the same line as in [7,17]. Introducing

$$k_{\tilde{\sigma}} = k\left(\frac{1+\tilde{\sigma}}{1+\tilde{\sigma}s^2}\right)^{1/2}, \quad k_{\tilde{\mu}} = k\left(\frac{1+\tilde{\mu}}{1+\tilde{\mu}s^2}\right)^{1/2}, \tag{29a,b}$$

and with the help of the identity

$$D_{k_1}(X) = D_{k_2}(X) + (k_1^2 - k_2^2)X, \tag{30}$$

the system (12a,b) takes the following form

$$(1+\tilde{\sigma}s^2) D_{k_{\tilde{\sigma}}}(B_r) = (\tilde{\sigma} - \tilde{\mu}) c k^2 (c B_r + s B_\theta) \tag{31a}$$

$$(1+\tilde{\mu}s^2) D_{k_{\tilde{\mu}}}(B_\theta) = (\tilde{\sigma} - \tilde{\mu}) c (s D_k(B_r) - c k^2 B_\theta). \tag{31b}$$

Then we can show that

$$D_{k_{\tilde{\mu}}}(c B_r + s B_\theta) = D_{k_{\tilde{\sigma}}}(s D_k(B_r) - c k^2 B_\theta) = 0. \tag{32a,b}$$

Then, using (32a,b) and (31a,b) leads to

$$(D_{k_{\tilde{\mu}}} \circ D_{k_{\tilde{\sigma}}})(B_r) = (D_{k_{\tilde{\sigma}}} \circ D_{k_{\tilde{\mu}}})(B_\theta) = 0. \tag{33a,b}$$

The two operators $D_{k_{\tilde{\sigma}}}$ and $D_{k_{\tilde{\mu}}}$ being commutative, B_r and B_θ satisfy the same linear differential equation of fourth order. As the solution of $D_\nu(X) = 0$ is a linear combination of $I_1(\nu r)$ and $K_1(\nu r)$, where I_1 and K_1 are first and second kind modified Bessel functions of order 1, the solutions of

(33a,b) are a linear combination of $I_1(k_{\tilde\sigma} r)$, $K_1(k_{\tilde\sigma} r)$, $I_1(k_{\tilde\mu} r)$ and $K_1(k_{\tilde\mu} r)$. Applying the boundary conditions (15a–d), B_r and B_θ can be written in the following form,

$$B_r = \begin{cases} r<1, & -s\left(\lambda_\sigma^R \dfrac{I_1(k_\sigma r)}{I_1(k_\sigma)} + \lambda_\mu^R \dfrac{I_1(k_\mu r)}{I_1(k_\mu)}\right) \\ 1<r<1+e & -s\left(\lambda_r^I \dfrac{I_1(kr)}{I_1(k)} + \lambda_r^K \dfrac{K_1(kr)}{K_1(k)}\right) \\ r>1+e, & -s\left(\lambda_\sigma^S \dfrac{K_1(k_\sigma r)}{K_1(k_\sigma(1+e))} + \lambda_\mu^S \dfrac{K_1(k_\mu r)}{K_1(k_\mu(1+e))}\right), \end{cases} \tag{34}$$

$$B_\theta = \begin{cases} r<1, & c\left(\lambda_\sigma^R \dfrac{I_1(k_\sigma r)}{I_1(k_\sigma)} + \dfrac{\mu s^2}{1+\mu s^2}\lambda_\mu^R \dfrac{I_1(k_\mu r)}{I_1(k_\mu)}\right) \\ 1<r<1+e, & c\left(\lambda_\theta^I \dfrac{I_1(kr)}{I_1(k)} + \lambda_\theta^K \dfrac{K_1(kr)}{K_1(k)}\right) \\ r>1+e, & c\left(\lambda_\sigma^S \dfrac{K_1(k_\sigma r)}{K_1(k_\sigma(1+e))} + \dfrac{\mu s^2}{1+\mu s^2}\lambda_\mu^S \dfrac{K_1(k_\mu r)}{K_1(k_\mu(1+e))}\right), \end{cases} \tag{35}$$

where B_θ has been obtained from B_r by replacing (34) in (31a). For $1<r<1+e$, the system (12a,b) leads to $D_k(B_r) = D_k(B_\theta) = 0$, and to the solutions (34b) and (35b).

In (34) and (35) there are eight unknowns: λ_σ^R and λ_μ^R related to the rotor, $\lambda_r^I, \lambda_r^K, \lambda_\theta^I$ and λ_θ^K related to the gap, λ_σ^S and λ_μ^S related to the stator. Therefore, to solve the problem we need eight equations. The six first ones are given by the boundary conditions (20)–(25), leading to

$$\lambda_r^I + \lambda_r^K = \lambda_\sigma^R + \lambda_\mu^R, \tag{36}$$

$$\varphi_\mu^{-1}\left(\lambda_\theta^I + \lambda_\theta^K\right) = \lambda_\sigma^R, \tag{37}$$

$$-k\varphi_\mu^{-1}\left(-\lambda_r^I \frac{I_0(k)}{I_1(k)} + \lambda_r^K \frac{K_0(k)}{K_1(k)}\right) = k_\sigma \lambda_\sigma^R \frac{I_0(k_\sigma)}{I_1(k_\sigma)} + k_\mu \lambda_\mu^R \frac{I_0(k_\mu)}{I_1(k_\mu)}. \tag{38}$$

$$\lambda_r^I \frac{I_1(k(1+e))}{I_1(k)} + \lambda_r^K \frac{K_1(k(1+e))}{K_1(k)} = \lambda_\sigma^S + \lambda_\mu^S, \tag{39}$$

$$\varphi_\mu^{-1}\left(\lambda_\theta^I \frac{I_1(k(1+e))}{I_1(k)} + \lambda_\theta^K \frac{K_1(k(1+e))}{K_1(k)}\right) = \lambda_\sigma^S, \tag{40}$$

$$k\varphi_\mu^{-1}\left(-\lambda_r^I \frac{I_0(k(1+e))}{I_1(k)} + \lambda_r^K \frac{K_0(k(1+e))}{K_1(k)}\right) = k_\sigma \lambda_\sigma^S \frac{K_0(k_\sigma(1+e))}{K_1(k_\sigma(1+e))} + k_\mu \lambda_\mu^S \frac{K_0(k_\mu(1+e))}{K_1(k_\mu(1+e))}. \tag{41}$$

Finally, to apply the two last boundary conditions (27) and (28), we need to calculate the z-component of the current density, that is given by

$$J_z = \tilde\varphi_\mu^{-1} \frac{1}{r}\frac{\partial}{\partial r}(r\tilde\phi), \quad \text{with } \tilde\phi = \tilde\mu c s B_r + (1+\tilde\mu s^2) B_\theta. \tag{42}$$

Replacing B_r and B_θ given by (34) and (35), in (42b) leads to

$$\tilde\phi = \begin{cases} r<1, & c\lambda_\sigma^R \dfrac{I_1(k_\sigma r)}{I_1(k_\sigma)} \\ 1<r<1+e, & c\left(\lambda_\theta^I \dfrac{I_1(kr)}{I_1(k)} + \lambda_\theta^K \dfrac{K_1(kr)}{K_1(k)}\right) \\ r>1+e, & c\lambda_\sigma^S \dfrac{K_1(k_\sigma r)}{K_1(k_\sigma(1+e))}, \end{cases} \tag{43}$$

which is nothing else than B_θ for $\mu = 0$, implying that $\boldsymbol{J}_z$ is not affected by the anisotropy of the magnetic permeability. Applying the relations $\partial_r(rI_1(\nu r)) = \nu r I_0(\nu r)$ and $\partial_r(rK_1(\nu r)) = -\nu r K_0(\nu r)$ to (42a), leads to

$$J_z = \begin{cases} r<1, & ck_\sigma \lambda_\sigma^R \dfrac{I_0(k_\sigma r)}{I_1(k_\sigma)} \\ 1<r<1+e, & ck\varphi_\mu^{-1}\left(\lambda_\theta^I \dfrac{I_0(kr)}{I_1(k)} - \lambda_\theta^K \dfrac{K_0(kr)}{K_1(k)}\right) \\ r>1+e, & -ck_\sigma \lambda_\sigma^S \dfrac{K_0(k_\sigma r)}{K_1(k_\sigma(1+e))}. \end{cases} \tag{44}$$

Replacing (34) and (44) in (27) and (28), leads to

$$\varphi_\sigma^{-1}\varphi_\mu^{-1} ck\left(\lambda_\theta^I \frac{I_0(k)}{I_1(k)} - \lambda_\theta^K \frac{K_0(k)}{K_1(k)}\right) - \omega s(\lambda_r^I + \lambda_r^K) = ck_\sigma \lambda_\sigma^R \frac{I_0(k_\sigma)}{I_1(k_\sigma)} - \Omega s(\lambda_\sigma^R + \lambda_\mu^R) \tag{45}$$

$$\begin{aligned} &\varphi_\sigma^{-1}\varphi_\mu^{-1} ck\left(\lambda_\theta^I \frac{I_0(k(1+e))}{I_1(k)} - \lambda_\theta^K \frac{K_0(k(1+e))}{K_1(k)}\right) - \omega s(1+e)\left(\lambda_r^I \frac{I_1(k(1+e))}{I_1(k)} + \lambda_r^K \frac{K_1(k(1+e))}{K_1(k)}\right) \\ &= -ck_\sigma \lambda_\sigma^S \frac{K_0(k_\sigma(1+e))}{K_1(k_\sigma(1+e))}. \end{aligned} \tag{46}$$

A dispersion relation can be derived, writing that the system composed of the eight equations (36)–(41), (45) and (46), with the eight unknowns $\lambda_\sigma^R, \lambda_\mu^R, \lambda_r^I, \lambda_r^K, \lambda_\theta^I, \lambda_\theta^K, \lambda_\sigma^S$ and λ_μ^S, is singular (zero determinant). It leads to the dynamo threshold Ω^c such that

$$\overline{\Omega^c} = \frac{F_\mu F_\sigma - \overline{\omega}[-M_{\mu\sigma}E_\mu E_\sigma + L_{\mu\sigma}(DBA' - BCB')]}{M_{\mu\sigma}(DBA' - BCB') - L_{\mu\sigma}(B' + K_\mu D)(B' + K_\sigma D) - M_{\mu\sigma}L_{\mu\sigma}D^2\overline{\omega}}, \tag{47}$$

with

$$\overline{\Omega^c} = \varphi_\mu\varphi_\sigma(\Omega^c - \omega)\frac{s}{c}, \quad \overline{\omega} = \varphi_\mu\varphi_\sigma\omega\frac{s}{c}(1+e), \quad A = \frac{I_0(k)}{I_1(k)}, \quad B = k\left(\frac{I_0(k)}{I_1(k)} + \frac{K_0(k)}{K_1(k)}\right), \tag{48}$$

$$C = \frac{I_1(k')}{I_1(k)}, \quad D = \frac{I_1(k')}{I_1(k)} - \frac{K_1(k')}{K_1(k)}, \quad A' = k\frac{I_0(k')}{I_1(k)}, \quad B' = k\left(\frac{I_0(k')}{I_1(k)} + \frac{K_0(k')}{K_1(k)}\right), \tag{49}$$

$$I_\mu = k_\mu\varphi_\mu\frac{I_0(k_\mu)}{I_1(k_\mu)}, \quad I_\sigma = k_\sigma\varphi_\sigma\frac{I_0(k_\sigma)}{I_1(k_\sigma)}, \quad K_\mu = k_\mu\varphi_\mu\frac{K_0(k'_\mu)}{K_1(k'_\mu)}, \quad K_\sigma = k_\sigma\varphi_\sigma\frac{K_0(k'_\sigma)}{K_1(k'_\sigma)}, \tag{50}$$

$$L_{\mu\sigma} = \varphi_\sigma^{-1}I_\sigma - \varphi_\mu^{-1}I_\mu, \quad M_{\mu\sigma} = \varphi_\sigma^{-1}K_\sigma - \varphi_\mu^{-1}K_\mu, \quad E_\mu = AD - BC - DI_\mu, \quad E_\sigma = AD - BC - DI_\sigma, \tag{51}$$

$$F_\mu = B(A' + K_\mu C) - (B' + K_\mu D)(A - I_\mu), \quad F_\sigma = B(A' + K_\sigma C) - (B' + K_\sigma D)(A - I_\sigma), \tag{52}$$

$$k' = (1+e)k, \quad k'_\mu = (1+e)k_\mu, \quad , k'_\sigma = (1+e)k_\sigma. \tag{53}$$

The derivation of (47) is given in Appendix A. At this stage we can make two checks, one for $e = 0$, the other for $e \to \infty$.

For $e = 0$, we have $k' = k$, $k'_\mu = k_\mu$, $k'_\sigma = k_\sigma$, $A' = A$, $B' = B$, $C = 1$, $D = 0$, $E_\mu = E_\sigma = -B$, $F_\mu = B(K_\mu + I_\mu)$, $F_\sigma = B(K_\sigma + I_\sigma)$. After some algebra and using the Wronskian relation $x((I_0(x))/(I_1(x)) + (K_0(x))/(K_1(x))) = [I_1(x)K_1(x)]^{-1}$, the following dynamo threshold is found

$$\Omega^c = \frac{c}{s}(I_1(k_\sigma)K_1(k_\sigma) - I_1(k_\mu)K_1(k_\mu))^{-1}, \tag{54}$$

which is nothing else than the expression given in [2].

In the limit $e \to \infty$, we have $k' \gg 1$, $k'_\mu \gg 1$, $k'_\sigma \gg 1$. Knowing that for $x \to \infty$, $I_0(x) \equiv I_1(x) \approx e^x/\sqrt{2\pi x} \to \infty$ and $K_0(x) \equiv K_1(x) \approx e^{-x}\sqrt{\pi/2x} \to 0$, we then have $B' \equiv A'$, $D \equiv C$, $K_\mu \equiv k_\mu\varphi_\mu$,

$K_\sigma \equiv k_\sigma \varphi_\sigma$, $M_{\mu\sigma} \equiv k_\sigma - k_\mu$. In (47), the factors multiplied by $\overline{\omega}$ are of the same order of magnitude as the terms that are not proportional to $\overline{\omega}$. As $\overline{\omega} \equiv e \gg 1$, Equation (47) then simplifies into

$$\overline{\Omega^c} = \frac{-M_{\mu\sigma} E_\mu E_\sigma + L_{\mu\sigma}(DBA' - BCB')}{M_{\mu\sigma} L_{\mu\sigma} D^2} \equiv \frac{-E_\mu E_\sigma}{L_{\mu\sigma} D^2}. \tag{55}$$

Then we can show that

$$\Omega^c - \omega = -\frac{c}{s} \frac{(\Phi(k_\sigma) + \varphi_\sigma^{-1}\Psi(k))(\Phi(k_\mu) + \varphi_\mu^{-1}\Psi(k))}{\Phi(k_\sigma) - \Phi(k_\mu)}, \tag{56}$$

where

$$\Phi(x) = xI_0(x)/I_1(x), \quad \Psi(x) = xK_0(x)/K_1(x), \tag{57a,b}$$

which is identical to the dynamo threshold expression given in [7] for a rotor immersed in an isotropic medium, both rotating at angular velocities Ω and ω respectively.

Finally, we note that in (47), exchanging σ and μ corresponds to changing the angular velocities $\overline{\Omega^c}$ and $\overline{\omega}$ into their opposite $-\overline{\Omega^c}$ and $-\overline{\omega}$, as already shown by [14,19] for the induction equation with isotropic electromagnetic conductivity and permeability.

In our model, ω is assumed to be constant with r. Therefore, taking $\omega = \beta\Omega$ with $\beta \in [0,1]$, and replacing in (47) leads to

$$\Omega^c = \frac{c}{s}\varphi_\sigma^{-1}\varphi_\mu^{-1} \frac{Q(1-\beta) + P(1+e)\beta \pm \sqrt{\Delta}}{2(1+e)\beta(1-\beta)M_{\mu\sigma}L_{\mu\sigma}D^2}, \tag{58}$$

with

$$P = [-M_{\mu\sigma}E_\mu E_\sigma + L_{\mu\sigma}(DBA' - BCB')], \tag{59}$$

$$Q = M_{\mu\sigma}(DBA' - BCB') - L_{\mu\sigma}(B' + K_\mu D)(B' + K_\sigma D), \tag{60}$$

$$\Delta = [Q(1-\beta) + P(1+e)\beta]^2 - 4F_\mu F_\sigma M_{\mu\sigma} L_{\mu\sigma} D^2 (1+e)\beta(1-\beta). \tag{61}$$

In the limit $\beta(1-\beta) \approx 0$, we have $|\Omega^c| \approx |(c/s)\varphi_\sigma^{-1}\varphi_\mu^{-1} F_\mu F_\sigma [Q(1-\beta) + P(1+e)\beta]^{-1}|$, leading to

$$|\Omega^c| = \begin{cases} \left|\frac{c}{s}\varphi_\sigma^{-1}\varphi_\mu^{-1} F_\mu F_\sigma Q^{-1}\right| \\ \left|\frac{c}{s}\varphi_\sigma^{-1}\varphi_\mu^{-1} F_\mu F_\sigma P^{-1}(1+e)^{-1}\right|, \end{cases} \qquad \text{for } \beta = \begin{cases} 0 \\ 1. \end{cases} \tag{62}$$

5. Results

As in [7], and with experimental applications in mind, we consider three cases characterized by the materials that compose both the rotor and the stator. The first case denoted copper$^{(\perp)}$/kapton$^{(\parallel)}$, corresponds to the choice made for the Fury dynamo experiment, in which the rotor and stator are composed of copper as the main conducting material and kapton as an electrical insulator. In Fury, vertical grooves have been cut following logarithmic spirals as in Figure 2. These grooves have been filled with kapton sheets to force the electrical currents to follow curved trajectories, in a way reproducing anisotropic electrical conductivity [1]. In the other two cases studied here, copper is replaced by iron or μ-metal, both of which have a relative magnetic permeability well in excess of unity. Kapton is replaced by tin, whose relative magnetic permeability is equal to unity. The resulting arrangements iron$^{(\perp)}$/tin$^{(\parallel)}$ and μ-metal$^{(\perp)}$/tin$^{(\parallel)}$ mimic materials with an anisotropic magnetic permeability. In all three cases the gap is filled with galinstan, an alloy of gallium, indium and tin, which is liquid at room temperature and essential for ensuring good electrical contact between the rotor and the stator. The values of the electrical conductivities and magnetic permeabilities corresponding to these three cases are collected in Table 1, together with the corresponding values of σ, μ, φ_σ and φ_μ.

Table 1. Electromagnetic properties of the materials composing the rotor, the gap and the stator

	Rotor/Stator						Gap (Galinstan)			
Materials	$\sigma^{\perp}$	$\mu^{\perp}$	$\sigma^{\parallel}$	$\mu^{\parallel}$	σ	μ	σ_g	μ_g	φ_σ	φ_μ
$Cu^{(\perp)}$ $Ka^{(\parallel)}$	63	1	5×10^{-22}	1	13×10^{22}	0	3.86	1	0.06	1
$Fe^{(\perp)}$ $Sn^{(\parallel)}$	10.2	5×10^{3}	9.9	1	0.03	5×10^{3}	3.86	1	0.38	2×10^{-4}
$\mu m^{(\perp)}$ $Sn^{(\parallel)}$	2.1	1.5×10^{5}	9.9	1	−0.79	1.5×10^{5}	3.86	1	1.85	6.7×10^{-6}

The electrical conductivities $\sigma^{\perp}$, $\sigma^{\parallel}$ and σ_g are given in unit of $10^6\ \Omega^{-1}\cdot\mathrm{m}^{-1}$. The magnetic permeabilities $\mu^{\perp}$, $\mu^{\parallel}$ and μ_g are given in unit of $4\pi\times10^{-7}$ H·m^{-1}. The parameters σ, μ, φ_σ and φ_μ are dimensionless. The numerical values of the electrical conductivity and magnetic permeability of the materials are taken from appropriate references [20–23].

Table 2. Geometrical characteristics of the Fury dynamo experiment [1] and another experimental project with larger galinstan gaps

	Dimensional				Dimensionless	
Parameters	R	e	h	α/π	e (%)	$k=2\pi R/h$
Units	cm	mm	cm	rad	–	–
Fury	5	0.5	20.9	0.15	1	1.5
Larger gap	7	2	30	0.15	2.9	1.5
		18			25.7	
		34			48.6	
		50			71.4	

The rotor's radius R, the gap thickness e, the height h of the experiment, are dimensional quantities. The pitch angle α of anisotropy is given in radian. The same notation e is used for the dimensional and dimensionless gap thickness, the relation between both being $e\,(\%) = 10^2(e/R)$. The value of k corresponds to a complete period of the magnetic field along the height of the experiment.

5.1. *Dimensionless results*

In Figure 3, the dynamo threshold Ω^c is plotted either (left) versus the magnetic wave number k for a pitch angle $\alpha/\pi = 0.15\pi$ or (right) versus α for $k = 1.5$. The three rows of subfigures correspond, from top to bottom, to the copper$^{(\perp)}$/kapton$^{(\parallel)}$, iron$^{(\perp)}$/tin$^{(\parallel)}$ and μ-metal$^{(\perp)}$/tin$^{(\parallel)}$ cases. In each subfigure six gap thicknesses e including the case without gap ($e = 0$), and three values of the angular velocities ratio β are considered. The value $e = 1\%$ corresponds to that of Fury. The other non-zero values of e correspond to larger gaps, up to 71.4% of the rotor radius. Table 2 summarises the geometric characteristics of Fury and those of a slightly larger model with several values of galinstan gap.

From the top subfigures of Figure 3 we see that, for $e = 2.9\%$, taking $\alpha = 0.15$ and $k = 0.15$ is not far from the minimum dynamo threshold. This is less true when e is increased. We could think that increasing the galinstan gap thickness is necessarily detrimental to the dynamo because the shear between the rotor and the stator will be weaker. This is mainly the case, except for example in the top left sub-figure, which shows curve crossings for $\beta = 0.5$, $e = 48.6\%$ and $e = 71.4\%$. Taking $\beta = 0$ leads to the largest dynamo threshold unless k is sufficiently large as can be seen e.g. at the top left subfigure, with curve crossings for $e = 71.4\%$, $\beta = 0.5$ and $\beta = 0$. We note that increasing e shifts the minimum threshold to smaller values of k and α.

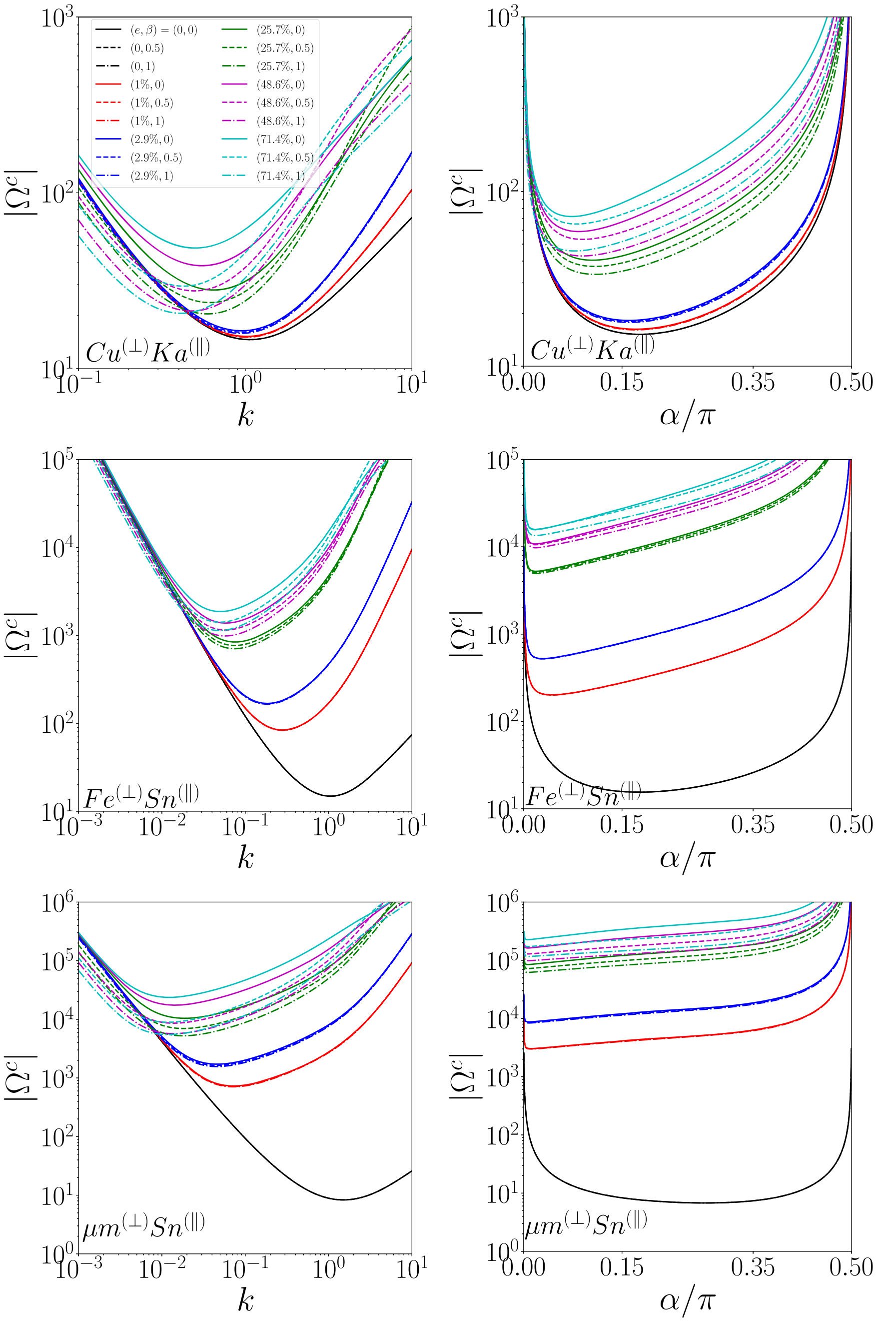

Figure 3. The dynamo threshold $|\Omega^c|$ is plotted, either (left) versus the wave number k for a pitch angle $\alpha = 0.15\pi$, or (right) versus α for $k = 1.5$. The top row corresponds to the copper$^{(\perp)}$/kapton$^{(\parallel)}$ case, the middle row to the iron$^{(\perp)}$/tin$^{(\parallel)}$ case, the bottom row to the μ-metal$^{(\perp)}$/tin$^{(\parallel)}$ case. Each curve corresponds to a couple (e,β), with $e \in \{0; 10^{-2}; 2.9\times 10^{-2}; 2.57\times 10^{-1}; 4.86\times 10^{-1}; 7.14\times 10^{-1};\}$ and $\beta \in \{0; 0.5; 1\}$.

Finally there is a stricking difference between the copper$^{(\perp)}$/kapton$^{(\parallel)}$ case and the two others iron$^{(\perp)}$/tin$^{(\parallel)}$ and μ-metal$^{(\perp)}$/tin$^{(\parallel)}$. Indeed, whereas at $e = 0$ the minimum dynamo thresholds of the three cases are comparable, $\min_k(\Omega^c(k)) \approx \{14.6, 14.8, 8.3\}$, increasing e leads to much higher dynamo thresholds for the two last cases, $\min_k(\Omega^c(k)) \approx \{15.1, 84, 710\}$ for $e = 1\%$, $\min_k(\Omega^c(k)) \approx \{16, 165, 1600\}$ for $e = 2.9\%$. This is presumably because in these cases the galinstan gap corresponds to an abrupt radial jump of the magnetic permeability, of at least four order of magnitude as given in Table 1 by the small values of φ_μ. In comparison, in the copper$^{(\perp)}$/kapton$^{(\parallel)}$ case, the radial jump of electrical conductivity of around two orders of magnitude as given by φ_σ in Table 1, is much less detrimental to the dynamo. This significant increase in the dynamo threshold for the cases of iron$^{(\perp)}$/tin$^{(\parallel)}$ and μ-metal$^{(\perp)}$/tin$^{(\parallel)}$ must however be revised when dimensional quantities are considered, as explained in Section 5.2.

In Figure 4 the electric current density and magnetic field lines are plotted at the threshold, in the three cases copper$^{(\perp)}$/kapton$^{(\parallel)}$, iron$^{(\perp)}$/tin$^{(\parallel)}$ and μ-metal$^{(\perp)}$/tin$^{(\parallel)}$, for $k = 1.5$, $\alpha/\pi = 0.15$, $\beta = 0$ and several values of e. The magnetic field lines are plotted from the expressions of B_r and B_θ given in (34) and (35). The electric current density can be calculated from (7c), leading to the dimensionless following expression

$$J_r = -\mathrm{i}k\tilde{\varphi}_\mu^{-1}\tilde{\phi}, \quad \text{with } \tilde{\phi} = \tilde{\mu}csB_r + (1+\tilde{\mu}s^2)B_\theta, \tag{63}$$

$$J_\theta = \mathrm{i}k^{-1}\tilde{\varphi}_\mu^{-1}[D_k(B_r) + \tilde{\mu}c^2k^2B_r + \tilde{\mu}csk^2B_\theta]. \tag{64}$$

At the dynamo threshold, $\gamma = 0$, Equation (12a) implies that

$$D_k(B_r) = (1+\tilde{\sigma}s^2)^{-1}[cs(\tilde{\sigma}-\tilde{\mu})k^2B_\theta - \tilde{\mu}c^2k^2B_r], \tag{65}$$

leading to

$$J_\theta = \mathrm{i}k\frac{cs\tilde{\sigma}}{1+s^2\tilde{\sigma}}\tilde{\varphi}_\mu^{-1}\tilde{\phi}. \tag{66}$$

Then (63) and (66) lead to the following relation

$$(1+s^2\tilde{\sigma})J_\theta + cs\tilde{\sigma}J_r = 0, \tag{67}$$

corresponding to logarithmic spiral lines for $\tilde{\sigma} \neq 0$ and radial lines for $\tilde{\sigma} = 0$ as plotted in Figure 4.

In Figure 5, $B_z(r)$ and $J_z(r)$ are plotted, again in the three cases copper$^{(\perp)}$/kapton$^{(\parallel)}$, iron$^{(\perp)}$/tin$^{(\parallel)}$ and μ-metal$^{(\perp)}$/tin$^{(\parallel)}$, and for the same parameters as in Figure 4. The expression of $J_z(r)$ is given in (44). The expression of $B_z(r)$ can be derived from (19). Applying the relations $\partial_r(rI_1(\nu r)) = \nu rI_0(\nu r)$ and $\partial_r(rK_1(\nu r)) = -\nu rK_0(\nu r)$ to (34), leads to

$$B_z = \mathrm{i}k^{-1}\begin{cases} r<1, & -s\left(\lambda_\sigma^R k_\sigma \dfrac{I_0(k_\sigma r)}{I_1(k_\sigma)} + \lambda_\mu^R k_\mu \dfrac{I_0(k_\mu r)}{I_1(k_\mu)}\right) \\ 1<r<1+e & -sk\left(\lambda_r^I \dfrac{I_0(kr)}{I_1(k)} - \lambda_r^K \dfrac{K_0(kr)}{K_1(k)}\right) \\ r>1+e, & s\left(\lambda_\sigma^S k_\sigma \dfrac{K_0(k_\sigma r)}{K_1(k_\sigma(1+e))} + \lambda_\mu^S k_\mu \dfrac{K_0(k_\mu r)}{K_1(k_\mu(1+e))}\right). \end{cases} \tag{68}$$

For $e = 0$, we can show from (38) and (41) that B_z given by (68) is continuous at $r = 1$, as plotted in Figure 5.

5.2. *Dimensional results*

In Figure 6, the critical frequency f^c is plotted versus the rotor's radius R for several values of the pitch angle α and of the gap thickness e (which after being multiplied by R is now dimensional). The magnetic wave number is fixed at $k = 1.5$, corresponding to an experiment with an aspect ratio $h/R = 2\pi/k$ of about 4.2, after assuming that the wavelength of the magnetic field is equal to the vertical size of the experiment. This aspect ratio of 4.2, which is the one used in Fury, is a

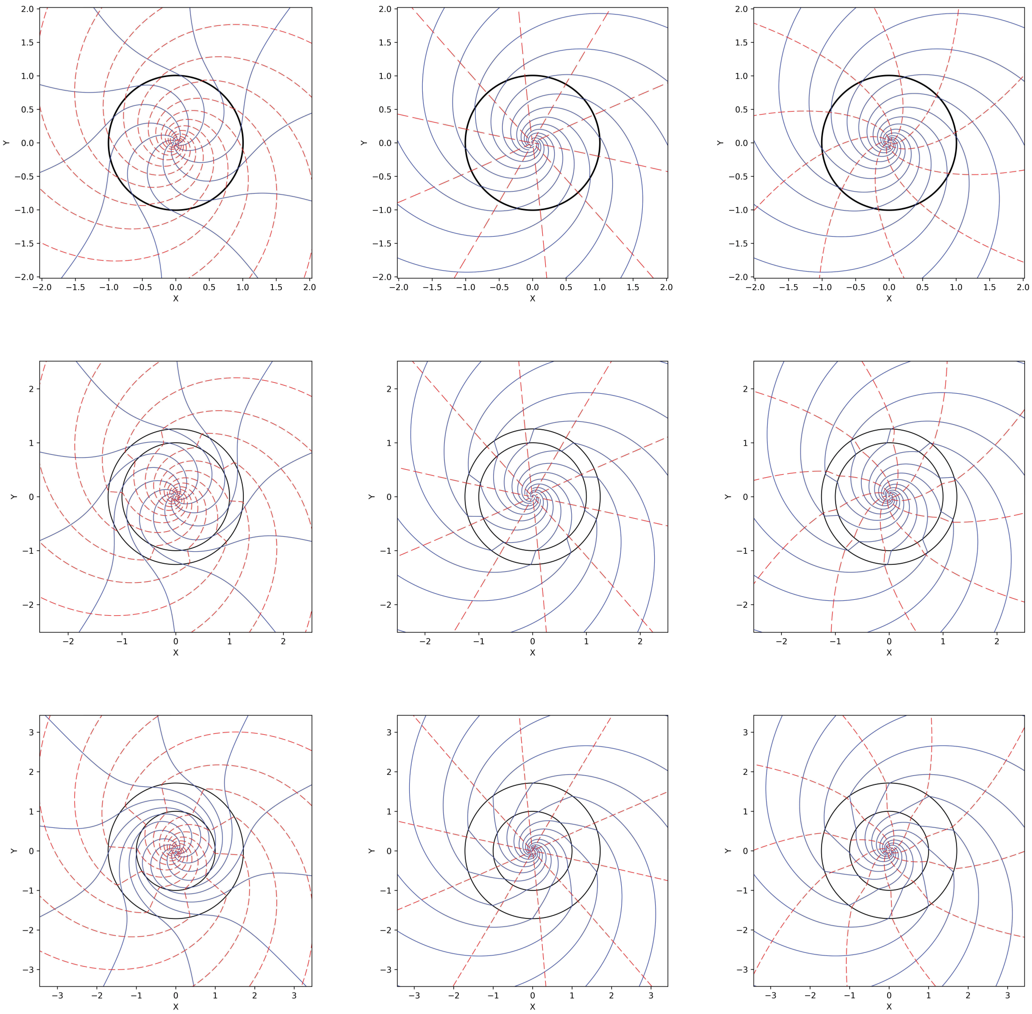

Figure 4. Plots of the magnetic field lines (full-blue) and the electric current lines (dashed-red) in the horizontal plane (x, y), for the three cases $\mathrm{Cu}^{(\perp)}\mathrm{Ka}^{(\parallel)}$ (left column), $\mathrm{Fe}^{(\perp)}$ $\mathrm{Sn}^{(\parallel)}$ (middle column), $\mu\mathrm{m}^{(\perp)}$ $\mathrm{Sn}^{(\parallel)}$ (right column), for $\alpha/\pi = 0.15$, $\beta = 0$, $k = 1.5$ and, from top to bottom, $e = 1\%, 25.7\%, 71.4\%$.

good compromise between theoretical predictions and the robustness of the device. The angular velocities ratio is fixed at $\beta = 0$, corresponding to a gap at rest. The frequency is obtained from

$$f^c = \frac{|\Omega^c|}{2\pi R^2 \sigma^\perp \mu^\perp}. \tag{69}$$

Taking $R = 7$ cm and $\alpha = 0.15\pi$ (solid lines), and for a rather large gap of galinstan $e = 50$ mm leads to a dynamo threshold $f^c = 35, 28$ and 14 Hz, for respectively the copper$^{(\perp)}$/kapton$^{(\parallel)}$, iron$^{\perp}$/tin$^{\parallel}$ and μ-metal$^{\perp}$/tin$^{\parallel}$ cases. These values are entirely achievable experimentally, and we note that the use of a galinstan gap with a rotor and stator of anisotropic magnetic permeability is not as detrimental as the dimensionless results suggested. It is even a much better system if a small rotor's radius is considered together with a small gap of galinstan. Indeed, for $R = 3$ cm and $e = 0.5$ mm, the dynamo threshold is $f^c = 1.3$ and 3 Hz for respectively the iron$^{\perp}$/tin$^{\parallel}$ and μ-metal$^{\perp}$/tin$^{\parallel}$ cases, whereas it is about 38 Hz for the copper$^{(\perp)}$/kapton$^{(\parallel)}$ case.

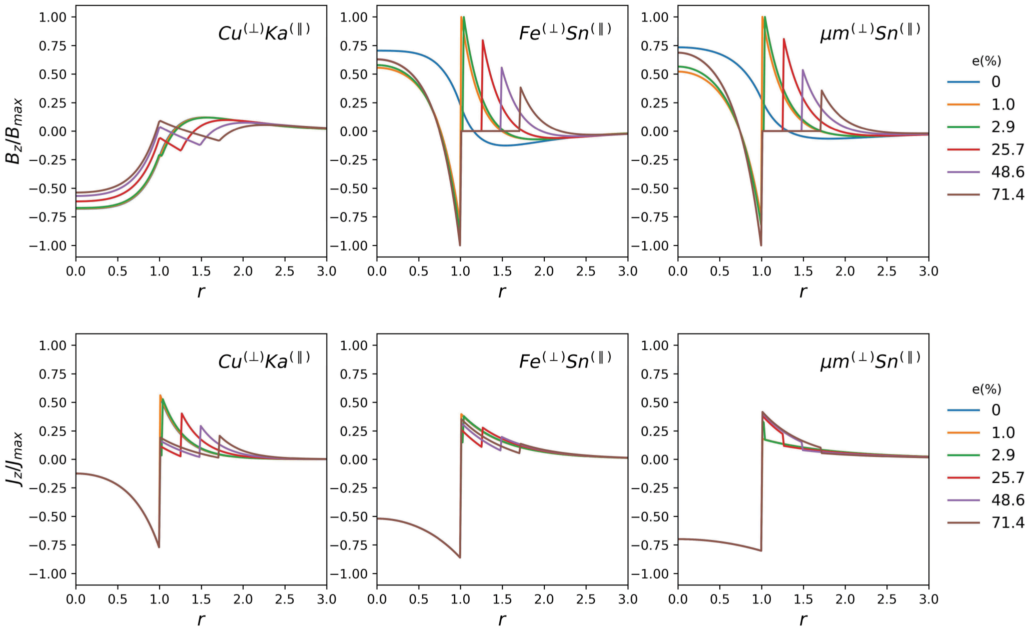

Figure 5. Plots of $B_z(r)/B_{\max}$ (top) and $J_z(r)/J_{\max}$ (bottom), for the three cases $\mathrm{Cu}^{(\perp)}\mathrm{Ka}^{(\parallel)}$ (left column), $\mathrm{Fe}^{(\perp)}$ $\mathrm{Sn}^{(\parallel)}$ (middle column), $\mu\mathrm{m}^{(\perp)}$ $\mathrm{Sn}^{(\parallel)}$ (right column), for $\alpha/\pi = 0.15$, $\beta = 0$, $k = 1.5$, and $e = 0\%, 1\%, 2.9\%, 25.7\%, 48.6\%, 71.4\%$.

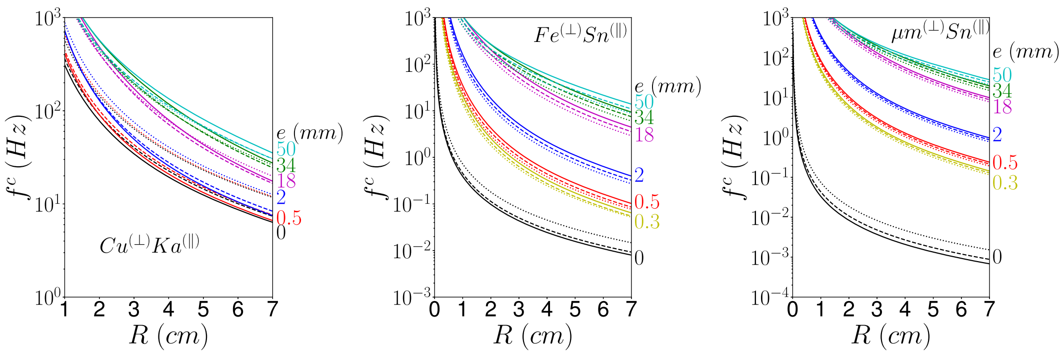

Figure 6. The critical frequency f^c (in Hz) is plotted versus the rotor's radius $R \in [0, 7$ cm] for (left) the copper$^\perp$/kapton$^\parallel$, (middle) the iron$^\perp$/tin$^\parallel$ and (right) the μ-metal$^\perp$/tin$^\parallel$ cases, with six or seven gap thicknesses $e \in [0, 50$ mm], and three values of α. The solid, dahed and dotted curves correspond to $\alpha/\pi = 0.15, 0.1, 0.05$. The wave number and angular velocities ratio are fixed at $k = 1.5$ and $\beta = 0$.

In the left subfigure of Figure 7, f^c is plotted versus e, for values of e and R smaller than the one used in Fury ($e \le 0.5$ mm and $R \le 3$ cm), $\beta = 0$ and $\alpha = 0.15\pi$. The results suggest the possibility of building a miniature dynamo with a rotor's radius R of 1–2 cm and a gap of galinstan e of 0.3 to 0.5 mm, using iron$^\perp$/tin$^\parallel$.

In the middle and right subfigures of Figure 7, f^c is plotted versus h in the iron$^\perp$/tin$^\parallel$ case, for $R = 1.5$ cm and $\beta = 0$. In the middle subfigure, e is varied and α is fixed to 0.15π, while in the right subfigure e is fixed to 0.3 mm and α is varied. In addition, two values of μ_g are considered,

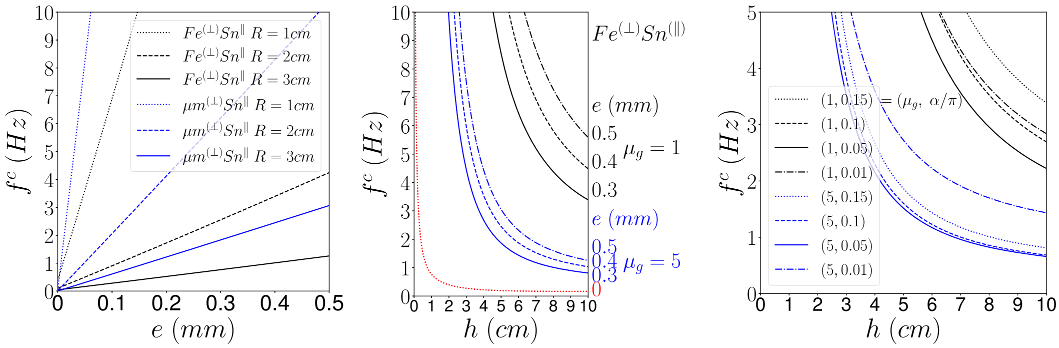

Figure 7. The critical frequency f^c (in Hz) is plotted: (left) versus the galinstan gap thickness e for the iron$^{\perp}$/tin$^{\parallel}$ and the μ-metal$^{\perp}$/tin$^{\parallel}$ cases, for three values of rotor's radius $R \in \{1,2,3\}$ cm, for $k = 1.5$ and $\alpha/\pi = 0.15$; (middle) versus the magnetic vertical wavelength h for the iron$^{\perp}$/tin$^{\parallel}$ case, for four values of gap's thickness $e \in \{0, 0.3, 0.4, 0.5\}$ mm, for $R = 1.5$ cm and $\alpha/\pi = 0.15$; (right) versus the magnetic vertical wavelength h for the iron$^{\perp}$/tin$^{\parallel}$ case, for four values of $\alpha/\pi \in \{0.01, 0.05, 0.1, 0.15\}$, for $R = 1.5$ cm and $e = 0.3$ mm. In all cases, $\beta = 0$. In the middle and right subfigures two values of μ_g are considered $\mu_g \in \{4\pi \times 10^{-7}, 20\pi \times 10^{-7}\}$.

Table 3. Dynamo threshold frequency for the iron$^{\perp}$/tin$^{\parallel}$ combination, $R = 1.5$ cm, $e = 0.3$ mm, two values of the pitch angle α, two values of the magnetic wave length h and two types of liquid metal filling the gap, galinstan or magnetic liquid metal

	$h = 10$ cm		$h = 5$ cm	
	f^c_{Ga} (Hz)	f^c_{MLM} (Hz)	f^c_{Ga} (Hz)	f^c_{MLM} (Hz)
$\alpha/\pi = 0.15$	3.4	0.8	8.5	1.9
$\alpha/\pi = 0.05$	2.2	0.7	6	1.5

either $\mu_g = 4\pi \times 10^{-7}$ H·m^{-1} for a gap filled with galinstan or $\mu_g = 20\pi \times 10^{-7}$ H·m^{-1} for a gap filled with a magnetic liquid metal (MLM) made of iron particules in liquid eGaIn. The electric conductivity of such MLM is equal to 3.9×10^6 Ω^{-1}·m^{-1}, so identical to the one of galinstan, but with a magnetic permeability five times larger [24].

From the middle subfigure of Figure 7 we see that for $e = 0.3$ mm and $h = 10$ cm the dynamo threshold is $f^c = 3.4$ Hz for a gap filled with galinstan, and $f^c = 0.8$ Hz for gap filled with MLM. Assuming that the stator's radius is twice larger than the rotor's radius $R = 1.5$ cm, the ensemble constituted of the rotor gap and stator will have a mass of about 2.2 kg (for an iron density equal to 7.86 g·cm^3). These results correspond to $\alpha/\pi = 0.15$.

From the right subfigure of Figure 7, wee see that taking smaller value of α down to $\alpha/\pi = 0.05$ leads to a smaller dynamo threshold. Therefore, for $R = 1.5$ cm, $e = 0.3$ mm and $\alpha/\pi = 0.05$, taking $h = 10$ cm leads to a dynamo threshold $f^c = 2.2$ Hz for a gap filled with galinstan, and $f^c = 0.7$ Hz for gap filled with MLM. This corresponds again to a device mass of about 2.2 kg. For a gap filled with MLM and device height $h = 5$ cm the dynamo threshold is about 1.5 Hz and the mass about 1.1 kg. The results are summarized in Table 3.

6. Conclusion

In this paper, we studied the presence of a gap between the rotor and stator of an anisotropic dynamo in cylindrical geometry. The rotor and the stator have a logarithmic anisotropy given by the same pitch angle α. The gap between the rotor and the stator is filled with an isotropic material, such as liquid metal. The dynamo threshold corresponding to the minimum angular velocity of the rotor, above which a magnetic field is generated, was calculated for different values of the gap thickness. We considered three cases depending on the materials composing both the rotor and stator, copper$^{\perp}$/kapton$^{\parallel}$, iron$^{\perp}$/tin$^{\parallel}$ and μ-metal$^{\perp}$/tin$^{\parallel}$, the first case corresponding to an electrical conductivity anisotropy, the two others to a magnetic permeability anisotropy. For the material filling the gap we mainly considered galinstan which is liquid at room temperature.

When the magnetic wavelength is not too large compared with the rotor radius, three general trends were found: (i) the presence of a gap is always detrimental to the dynamo, and (ii) the most detrimental case corresponds to a gap at rest, which is therefore the case selected for dimensioning a new experimental application, (iii) increasing the gap thickness increases the dynamo threshold.

The study focused more specifically on two objectives. The first one concerns the dimensioning of a new experiment with a gap larger than that of Fury so that, once the dynamo is established, it can react dynamically with the flow within the gap by means of Lorentz forces. But of course, to do this, we first need to be able to start a dynamo with a large gap. Although the copper$^{\perp}$/kapton$^{\parallel}$ combination appears as slightly less interesting than the other two, it still offers reasonable values of the dynamo threshold, with rotor's frequencies f^c between 10Hz and 35 Hz for a rotor's radius $R = 7$ cm and a gap thickness e between 0.2 cm and 5 cm. By way of comparison, in the case of Fury, the dynamo threshold frequency was f^c =24 Hz (for $R = 5$ cm, $h = 20.9$ cm and $e = 0.5$ mm). Assuming a rotor radius $R = 7$ cm and a height h =30 cm (corresponding to $k = 1.5$ as in Fury), a gap thickness $e = 5$ cm and a stator thickness of 4 cm, with copper and galinstan densities of 9 g·cm^{-3} and 6.44 g·cm^{-3} respectively, we obtain a mass of about 200 kg, almost five times heavier than Fury but nevertheless achievable on a laboratory scale. The advantage of such copper$^{\perp}$/kapton$^{\parallel}$ combination is that it precisely does not contain any magnetic material garanteeing a dynamo starting without any help of a remanent magnetic field contrary to previous experiments [25]. In addition, Fury has demonstrated experimentally that such a combination works like a dynamo, at least for a thin galinstan gap. At the moment no anisotropic dynamo experiment based on iron$^{\perp}$/tin$^{\parallel}$ or μ-metal$^{\perp}$/tin$^{\parallel}$ has yet been built. This brings us to our second objective, which is to build a miniature dynamo experiment with a mass of the order of one kilogram.

To design a miniature dynamo experiment, we need to reduce the rotor radius, its height and the gap thickness. Of the three combinations studied, the iron$^{\perp}$/tin$^{\parallel}$ combination appears to be the most appropriate with the lowest dynamo threshold. Assuming a rotor radius $R = 1.5$ cm, a height $h = 10$ cm (corresponding to $k = 0.94$), and a galinstan gap thickness $e = 0.3$ mm, the dynamo threshold corresponds to a rotor frequency $f^c = 2.2$ Hz (resp. 3.4 Hz) for an anisotropic pitch angle $\alpha/\pi = 0.05$ (resp. 0.15). For a stator thickness of 1.5 cm and an iron density of 7.86 g·cm^{-1}, we obtain a mass of about 2.2 kg. If, instead of galinstan, the gap is filled with a magnetic liquid metal made up of iron particles in liquid eGaIn, the height and mass of the experiment can even be divided by a factor of 2, corresponding to a mass around 1.1 kg, and a dynamo threshold rotor frequency $f^c = 1.5$ Hz for $\alpha/\pi = 0.05$.

Declaration of interests

The authors do not work for, advise, own shares in, or receive funds from any organization that could benefit from this article, and have declared no affiliations other than their research organizations.

Funding

FP acknowledges the French Academy of Sciences and Electricité de France for granting the Ampère prize to the ISTerre Geodynamo team in 2021. This work was supported by the PEPR Origins.

Appendix A.

The matrix obtained from Equations (36)–(41), (45) and (46) is written below, with the following order of the variables λ_σ^R, λ_μ^R, λ_r^I, λ_r^K, λ_θ^I, λ_θ^K, λ_σ^S and λ_μ^S, using the following notations

$$\begin{aligned}
A &= k\frac{I_0(k)}{I_1(k)}, \quad B = k\left(\frac{I_0(k)}{I_1(k)} + \frac{K_0(k)}{K_1(k)}\right),\\
A' &= k\frac{I_0(k')}{I_1(k)}, \quad B' = k\left(\frac{I_0(k')}{I_1(k)} + \frac{K_0(k')}{K_1(k)}\right),\\
C &= \frac{I_1(k')}{I_1(k)}, \quad D = \frac{I_1(k')}{I_1(k)} - \frac{K_1(k')}{K_1(k)},\\
I_\mu &= k_\mu\varphi_\mu\frac{I_0(k_\mu)}{I_1(k_\mu)}, \quad I_\sigma = k_\sigma\varphi_\sigma\frac{I_0(k_\sigma)}{I_1(k_\sigma)},\\
K_\mu &= k_\mu\varphi_\mu\frac{K_0(k'_\mu)}{K_1(k'_\mu)}, \quad K_\sigma = k_\sigma\varphi_\sigma\frac{K_0(k'_\sigma)}{K_1(k'_\sigma)}.
\end{aligned}$$

The system that must be singular (zero determinant) is thus represented by the matrix

$$\begin{matrix}
-1 & -1 & 1 & 1 & 0 & 0 & 0 & 0\\
-1 & 0 & 0 & 0 & \varphi_\mu^{-1} & \varphi_\mu^{-1} & 0 & 0\\
-\varphi_\sigma^{-1}I_\sigma & -\varphi_\mu^{-1}I_\mu & \varphi_\mu^{-1}A & -\varphi_\mu^{-1}(B-A) & 0 & 0 & 0 & 0\\
0 & 0 & C & C-D & 0 & 0 & -1 & -1\\
0 & 0 & 0 & 0 & \varphi_\mu^{-1}C & \varphi_\mu^{-1}(C-D) & -1 & 0\\
0 & 0 & -\varphi_\mu^{-1}A' & \varphi_\mu^{-1}(B'-A') & 0 & 0 & -\varphi_\sigma^{-1}K_\sigma & -\varphi_\mu^{-1}K_\mu\\
-c\varphi_\sigma^{-1}I_\sigma+\Omega s & \Omega s & -\omega s & -\omega s & \varphi_\sigma^{-1}\varphi_\mu^{-1}cA & -\varphi_\sigma^{-1}\varphi_\mu^{-1}c(B-A) & 0 & 0\\
0 & 0 & -\omega s(1+e)C & -\omega s(1+e)(C-D) & \varphi_\sigma^{-1}\varphi_\mu^{-1}cA' & -\varphi_\sigma^{-1}\varphi_\mu^{-1}c(B'-A') & c\varphi_\sigma^{-1}K_\sigma & 0.
\end{matrix}$$

Let's modify the matrix in the following ways: exchange column 1 and 2 (the determinant is opposite), replace column 2 by 1-2 (the determinant is opposite), replace column 4 by 4-3 (no change in the determinant), multiply columns 3, 4, 5 and 6 by φ_μ (the determinant is multiplied by φ_μ^4), replace column 6 by 6-5 (no change in the determinant), replace column 7 by 8-7 (the determinant is opposite), add φ_μ times column 1 to column 3 (no change in the determinant), divide lines 7 and 8 by c (the determinant is divided by c^2), replace column 5 by 5-2 (no change in the determinant) and multiply lines 7 and 8 by φ_σ (the determinant is multiplied by φ_σ^2). We now have the matrix

$$\begin{matrix}
-1 & 0 & 0 & 0 & 0 & 0 & 0 & 0\\
0 & 1 & 0 & 0 & 0 & 0 & 0 & 0\\
-\varphi_\mu^{-1}I_\mu & \varphi_\sigma^{-1}I_\sigma-\varphi_\mu^{-1}I_\mu & A-I_\mu & -B & -\varphi_\sigma^{-1}I_\sigma+\varphi_\mu^{-1}I_\mu & 0 & 0 & 0\\
0 & 0 & \varphi_\mu C & -\varphi_\mu D & 0 & 0 & 0 & -1\\
0 & 0 & 0 & 0 & C & -D & 1 & 0\\
0 & 0 & -A' & B' & 0 & 0 & \varphi_\sigma^{-1}K_\sigma-\varphi_\mu^{-1}K_\mu & -\varphi_\mu^{-1}K_\mu\\
\varphi_\sigma\Omega\frac{s}{c} & I_\sigma & \varphi_\mu\varphi_\sigma(\Omega-\omega)\frac{s}{c} & 0 & A-I_\sigma & -B & 0 & 0\\
0 & 0 & -\varphi_\mu\varphi_\sigma\omega\frac{s}{c}(1+e)C & \varphi_\mu\varphi_\sigma\omega\frac{s}{c}(1+e)D & A' & -B' & -K_\sigma & 0.
\end{matrix}$$

Its determinant is $-c^{-2}\varphi_\mu^4\varphi_\sigma^2$ times the original determinant. With an opposite sign, it is also the determinant of the 6×6 bottom-right sub-matrix

$$\begin{array}{cccccc}
A-I_\mu & -B & -\varphi_\sigma^{-1}I_\sigma+\varphi_\mu^{-1}I_\mu & 0 & 0 & 0\\
\varphi_\mu C & -\varphi_\mu D & 0 & 0 & 0 & -1\\
0 & 0 & C & -D & 1 & 0\\
-A' & B' & 0 & 0 & \varphi_\sigma^{-1}K_\sigma-\varphi_\mu^{-1}K_\mu & -\varphi_\mu^{-1}K_\mu\\
\varphi_\mu\varphi_\sigma(\Omega-\omega)\dfrac{s}{c} & 0 & A-I_\sigma & -B & 0 & 0\\
-\varphi_\mu\varphi_\sigma\omega\dfrac{s}{c}(1+e)C & \varphi_\mu\varphi_\sigma\omega\dfrac{s}{c}(1+e)D & A' & -B' & -K_\sigma & 0.
\end{array}$$

We introduce some more notations

$$\begin{aligned}
L_{\mu\sigma} &= k_\sigma\frac{I_0(k_\sigma)}{I_1(k_\sigma)}-k_\mu\frac{I_0(k_\mu)}{I_1(k_\mu)}=\varphi_\sigma^{-1}I_\sigma-\varphi_\mu^{-1}I_\mu,\\
M_{\mu\sigma} &= k_\sigma\frac{K_0(k'_\sigma)}{K_1(k'_\sigma)}-k_\mu\frac{K_0(k'_\mu)}{K_1(k'_\mu)}=\varphi_\sigma^{-1}K_\sigma-\varphi_\mu^{-1}K_\mu,\\
\overline{\Omega} &= \varphi_\mu\varphi_\sigma(\Omega-\omega)\frac{s}{c},\\
\overline{\omega} &= \varphi_\mu\varphi_\sigma\omega\frac{s}{c}(1+e),
\end{aligned}$$

and the matrix can be written

$$\begin{array}{cccccc}
A-I_\mu & -B & -L_{\mu\sigma} & 0 & 0 & 0\\
\varphi_\mu C & -\varphi_\mu D & 0 & 0 & 0 & -1\\
0 & 0 & C & -D & 1 & 0\\
-A' & B' & 0 & 0 & M_{\mu\sigma} & -\varphi_\mu^{-1}K_\mu\\
\overline{\Omega} & 0 & A-I_\sigma & -B & 0 & 0\\
-\overline{\omega}C & \overline{\omega}D & A' & -B' & -K_\sigma & 0.
\end{array}$$

Removing $\varphi_\mu^{-1}K_\mu$ times line 2 to line 4, leads to the matrix

$$\begin{array}{cccccc}
A-I_\mu & -B & -L_{\mu\sigma} & 0 & 0 & 0\\
\varphi_\mu C & -\varphi_\mu D & 0 & 0 & 0 & -1\\
0 & 0 & C & -D & 1 & 0\\
-A'-K_\mu C & B'+K_\mu D & 0 & 0 & M_{\mu\sigma} & 0\\
\overline{\Omega} & 0 & A-I_\sigma & -B & 0 & 0\\
-\overline{\omega}C & \overline{\omega}D & A' & -B' & -K_\sigma & 0.
\end{array}$$

Its determinant is just opposite to the determinant of the 5×5 sub-matrix obtained when developing the last column

$$\begin{array}{ccccc}
A-I_\mu & -B & -L_{\mu\sigma} & 0 & 0\\
0 & 0 & C & -D & 1\\
-A'-K_\mu C & B'+K_\mu D & 0 & 0 & M_{\mu\sigma}\\
\overline{\Omega} & 0 & A-I_\sigma & -B & 0\\
-\overline{\omega}C & \overline{\omega}D & A' & -B' & -K_\sigma.
\end{array}$$

Removing $M_{\mu\sigma}$ times the second line to the third and $-K_\sigma$ times the second line to the fifth, the determinant is equal to that of the 4×4 submatrix

$$\begin{array}{cccc}
A-I_\mu & -B & -L_{\mu\sigma} & 0\\
-A'-K_\mu C & B'+K_\mu D & -M_{\mu\sigma}C & M_{\mu\sigma}D\\
\overline{\Omega} & 0 & A-I_\sigma & -B\\
-\overline{\omega}C & \overline{\omega}D & A'+K_\sigma C & -B'-K_\sigma D.
\end{array}$$

Adding $M_{\mu\sigma}DB^{-1}$ times the third line to the second line, then adding $B^{-1}(-B'-K_\sigma D)$ times the third line to the fourth line, leads to the determinant of a 3×3 submatrix

$$\begin{matrix} A-I_\mu & -B & -L_{\mu\sigma} \\ -A'-K_\mu C+M_{\mu\sigma}DB^{-1}\overline{\Omega} & B'+K_\mu D & -M_{\mu\sigma}(C-(A-I_\sigma)DB^{-1}) \\ -\overline{\omega}C-(B'+K_\sigma D)B^{-1}\overline{\Omega} & \overline{\omega}D & A'+K_\sigma C-(B'+K_\sigma D)B^{-1}(A-I_\sigma). \end{matrix}$$

Adding $(A-I_\mu)B^{-1}$ times the second column to the first column and subtracting $L_{\mu\sigma}B^{-1}$ times the second column to the third column, leads to the 2×2 submatrix

$$\begin{matrix} -A'-K_\mu C+M_{\mu\sigma}DB^{-1}\overline{\Omega}+(A-I_\mu)B^{-1}(B'+K_\mu D) & -M_{\mu\sigma}(C-(A-I_\sigma)DB^{-1})-L_{\mu\sigma}B^{-1}(B'+K_\mu D) \\ -\overline{\omega}C-(B'+K_\sigma D)B^{-1}\overline{\Omega}+(A-I_\mu)B^{-1}\overline{\omega}D & A'+K_\sigma C-(B'+K_\sigma D)B^{-1}(A-I_\sigma)-L_{\mu\sigma}B^{-1}\overline{\omega}D. \end{matrix}$$

Multiplying all coefficients by B and rearranging leads to

$$\begin{matrix} -A'B-K_\mu BC+M_{\mu\sigma}D\overline{\Omega}+(A-I_\mu)(B'+K_\mu D) & M_{\mu\sigma}(-BC+AD-I_\sigma D)-L_{\mu\sigma}(B'+K_\mu D) \\ -(B'+K_\sigma D)\overline{\Omega}+(AD-I_\mu D-BC)\overline{\omega} & B(A'+K_\sigma C)-(B'+K_\sigma D)(A-I_\sigma)-L_{\mu\sigma}D\overline{\omega}. \end{matrix}$$

We introduce the following last notations

$$\begin{aligned} E_\mu &= AD-BC-DI_\mu, \quad E_\sigma = AD-BC-DI_\sigma, \\ F_\mu &= B(A'+K_\mu C)-(B'+K_\mu D)(A-I_\mu), \quad F_\sigma = B(A'+K_\sigma C)-(B'+K_\sigma D)(A-I_\sigma), \end{aligned}$$

so that the 2×2 matrix can be written

$$\begin{matrix} -F_\mu+M_{\mu\sigma}D\overline{\Omega} & E_\sigma M_{\mu\sigma}-L_{\mu\sigma}(B'+K_\mu D) \\ -(B'+K_\sigma D)\overline{\Omega}+E_\mu\overline{\omega} & F_\sigma-L_{\mu\sigma}D\overline{\omega}. \end{matrix}$$

Its determinant can be readily calculated

$$\begin{aligned} \det = & -F_\mu F_\sigma+\overline{\Omega}[M_{\mu\sigma}(DF_\sigma+B'E_\sigma+K_\sigma DE_\sigma)-L_{\mu\sigma}(B'+K_\mu D)(B'+K_\sigma D)] \\ & +\overline{\omega}[-M_{\mu\sigma}E_\mu E_\sigma+L_{\mu\sigma}(DF_\mu+B'E_\mu+K_\mu DE_\mu)]-M_{\mu\sigma}L_{\mu\sigma}D^2\overline{\Omega}\overline{\omega}. \end{aligned}$$

Now, we remark that the coefficients we have introduced are not independent and we have

$$\begin{aligned} DF_\sigma+B'E_\sigma+K_\sigma DE_\sigma &= DBA'-BCB', \\ DF_\mu+B'E_\mu+K_\mu DE_\mu &= DBA'-BCB', \end{aligned}$$

making these two combinations equal and independent of σ or μ. So the determinant is now

$$\begin{aligned} \det = & -F_\mu F_\sigma+\overline{\Omega}[M_{\mu\sigma}(DBA'-BCB')-L_{\mu\sigma}(B'+K_\mu D)(B'+K_\sigma D)] \\ & +\overline{\omega}[-M_{\mu\sigma}E_\mu E_\sigma+L_{\mu\sigma}(DBA'-BCB')]-M_{\mu\sigma}L_{\mu\sigma}D^2\overline{\Omega}\overline{\omega}. \end{aligned}$$

Because $M_{\mu\sigma}$ and $L_{\mu\sigma}$ are both antisymmetrical (they change sign when σ and μ are switched), we can see that the determinant obeys the symmetry

$$\det(\mu,\sigma,\overline{\Omega},\overline{\omega}) = \det(\sigma,\mu,-\overline{\Omega},-\overline{\omega}).$$

References

[1] T. Alboussière, F. Plunian and M. Moulin, "Fury: an experimental dynamo with anisotropic electrical conductivity", *Proc. R. Soc. Lond. A* **478** (2022), article no. 20220374.

[2] F. Plunian and T. Alboussière, "Axisymmetric dynamo action produced by differential rotation, with anisotropic electrical conductivity and anisotropic magnetic permeability", *J. Plasma Phys.* **87** (2021), no. 1, article no. 905870110.

[3] A. Gailitis, O. Lielausis, E. Platacis, et al., "Magnetic field saturation in the Riga dynamo experiment", *Phys. Rev. Lett.* **86** (2001), pp. 3024–3027.

[4] R. Stieglitz and U. Müller, "Experimental demonstration of a homogeneous two-scale dynamo", *Phys. Fluids* **13** (2001), no. 3, pp. 561–564.

[5] R. Monchaux, M. Berhanu, M. Bourgoin, et al., "Generation of a magnetic field by dynamo action in a turbulent flow of liquid sodium", *Phys. Rev. Lett.* **98** (2007), article no. 044502.

[6] F. Ravelet, M. Berhanu, R. Monchaux, et al., "Chaotic dynamos generated by a turbulent flow of liquid sodium", *Phys. Rev. Lett.* **101** (2008), article no. 074502.
[7] F. Plunian and T. Alboussière, "Dynamo action produced by an anisotropic rotor immersed in an electrically conducting medium at rest", *Phys. Rev. Fluids* **8** (2023), article no. 113702.
[8] D. P. Lathrop and C. B. Forest, "Magnetic dynamos in the lab", *Phys. Today* **64** (2011), no. 7, pp. 40–45.
[9] F. Stefani, T. Albrecht, G. Gerbeth, A. Giesecke, T. Gundrum, J. Herault, C. Nore and C. Steglich, "Towards a precession driven dynamo experiment", *Magnetohydrodynamics* **51** (2015), no. 2, pp. 275–284.
[10] F. H. Busse and J. Wicht, "A simple dynamo caused by conductivity variations", *Geophys. Astrophys. Fluid Dyn.* **64** (1992), no. 1–4, pp. 135–144.
[11] B. Gallet, F. Pétrélis and S. Fauve, "Dynamo action due to spatially dependent magnetic permeability", *Europhys. Lett.* **97** (2012), no. 6, article no. 69001.
[12] B. Gallet, F. Pétrélis and S. Fauve, "Spatial variations of magnetic permeability as a source of dynamo action", *J. Fluid Mech.* **727** (2013), pp. 161–190.
[13] F. Pétrélis, A. Alexakis and C. Gissinger, "Fluctuations of electrical conductivity: a new source for astrophysical magnetic fields", *Phys. Rev. Lett.* **116** (2016), article no. 161102.
[14] F. Marcotte, B. Gallet, F. Pétrélis and C. Gissinger, "Enhanced dynamo growth in nonhomogeneous conducting fluids", *Phys. Rev. E* **104** (2021), article no. 015110.
[15] M. S. Ruderman and A. A. Ruzmaikin, "Magnetic field generation in an anisotropically conducting fluid", *Geophys. Astrophys. Fluid Dyn.* **28** (1984), no. 1, pp. 77–88.
[16] F. Plunian and T. Alboussière, "Axisymmetric dynamo action is possible with anisotropic conductivity", *Phys. Rev. Res.* **2** (2020), article no. 013321.
[17] F. Plunian and T. Alboussière, "Fast and Furious dynamo action in the anisotropic dynamo", *J. Fluid Dyn.* **87** (2022), article no. A66.
[18] T. Alboussière, K. Drif and F. Plunian, "Dynamo action in sliding plates of anisotropic electrical conductivity", *Phys. Rev. E* **101** (2020), article no. 033107.
[19] B. Favier and M. R. E. Proctor, "Growth rate degeneracies in kinematic dynamos", *Phys. Rev. E* **88** (2013), article no. 031001.
[20] D. Jiles, *Introduction to Magnetism and Magnetic materials*, Springer: New York, 1991.
[21] W. F. Gale and T. C. Totemeir, *Smithells Metal Reference Book*, Elsevier: Amsterdam, 2004.
[22] J. Wu and D. D. L. Chung, "Combined use of magnetic and electrically conductive fillers in a polymer matrix for electromagnetic interference shielding", *J. Electron. Mater.* **37** (2008), pp. 1088–1094.
[23] DuPont de Nemours, *Summary of Properties*, 2022. Online at https://www.dupont.com/content/dam/electronics/amer/us/en/electronics/public/documents/en/EI-10142_Kapton-Summary-of-Properties.pdf (accessed March 23, 2025).
[24] F. Carle, K. Bai, J. Casara, K. Vanderlick and E. Brown, "Development of magnetic liquid metal suspensions for magnetohydrodynamics", *Phys. Rev. Fluids* **2** (2017), article no. 013301.
[25] S. Miralles, N. Bonnefoy, M. Bourgoin, et al., "Dynamo threshold detection in the von Kármán sodium experiment", *Phys. Rev. E* **88** (2013), article no. 013002.